VOLUME 120, NUMBER 6
FEBRUARY 18, 1998

JOURNAL OF THE AMERICAN CHEMICAL SOCIETY

Nanosecond Molecular Dynamics of Hybrid Triplex and Duplex of Polycation Deoxyribonucleic Guanidine Strands with a Complimentary DNA Strand

Jia Luo and Thomas C. Bruice*

Contribution from the Department of Chemistry, University of California at Santa Barbara, Santa Barbara, California 93106

Received September 23, 1997

Abstract: Replacement of the phosphodiester linkages of the polyanion DNA with guanidinium linkers provides the polycation deoxyribonucleic guanidine (DNG). Molecular dynamics studies to 1120 ps of the hybrid triplex and 1420 ps of the hybrid duplex formed from octameric DNG strands $d(Tg)_8$ with a complementary DNA oligomer strand $d(Ap)_8$ have been carried out with water explicitly as solvent and Na^+Cl^- as counterions under periodic boundary conditions using the CHARMM force field and Ewald summation method. The Watson−Crick and Hoogstein hydrogen-bonding patterns of the A/T tracts remained intact without any structural restraints for both hybrid duplex and triplex structures throughout the simulation. And for the hybrid duplex and triplex structures, both 5′ and 3′ ends were only partially frayed. In agreement with our previous thermodynamic study the hybrid triplex is more favorable than the hybrid duplex in the simulations. This conclusion is reached by the comparison of the extent of 5′ end fraying and the bifurcating properties of the two systems. The structural histories of the DNG·DNA·DNG triplex and DNG·DNA duplex were determined by examining histograms from the last 1400 ps (duplex) and 1100 ps (triplex) of the dynamics run. These include the hydrogen-bonding pattern (sequence recognition) and base pair opening occurrences, minor groove width narrowing, and tract bending for the hybrid duplex and triplex structures. The bending angle measured between the local axis vectors of the first and last helical axis segments is about 30° for the averaged structures of both hybrid duplex and Watson−Crick portion of the hybrid triplex. Propeller twist (associated with three centered hydrogen bonding) up to −30°, native to DNA AT base pairing, was also observed for the duplex structure. The helical rise and twist parameters of the duplex structure and the duplex portion of the triplex structure assume a more B-DNA like conformation. However, the sugar pucker and other helical, axis, and base pair parameters of the two structures equilibrate at a A and B complex conformation, from base to base and base pair to base pair, which suggests a more A-DNA like overall conformation. Water spines are observed during the dynamics runs for both hybrid duplex and triplex structures in both minor and major grooves. The counterions remain in their positions through the dynamics run for the triplex system.

Introduction

Replacement of the phosphodiester linkages of a polyanion DNA/RNA with guanidine linkers provides a polycationic deoxyribonucleic/ribonucleic guanidine (DNG/RNG).[1−6] DNG/RNG's are novel new materials with promise in biological research and as sources of putative drugs. (Chart 1 shows the DNG oligomer of importance in the present investigation.) Oligonucleotide analogues capable of arresting cellular processes at the translational and transcriptional levels via specific sequence recognitions of RNA and DNA, respectively, are known as antisense and antigene agents.[7−11] Key goals in the design of such agents include increased binding ability to nucleic

S0002-7863(97)03337-4 CCC: $15.00
Published on Web 01/30/1998

Chart 1

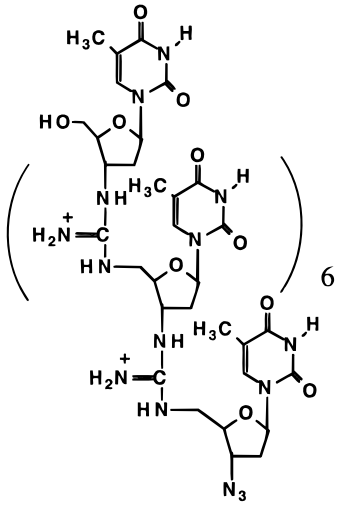

acid receptors with fidelity of sequence recognition, resistance to the degradation by nucleases, and increased membrane permeability. Replacement of the phosphodiester linkages with the guanido linker renders the resultant structures impervious to nuclease attack. This substitution leaves Watson−Crick base-pairing interactions intact and provides additional electrostatic attractions with targeted nucleic acid. The positive charge of the linker [−NH−C(=N^+H_2)−NH−] of DNG has an electrostatic attraction to the negative phosphodiester [−O−(PO_2−)−O−] linker of DNA or RNA. Moreover, a DNG complex with a complementary strand of either DNA or RNA will exhibit a net neutral charge, a feature which should facilitate cellular uptake. Our previous thermodynamic studies showed that a pentameric thymidyl DNG, $d(Tg)_4$-T-azido, is specific for its complementary tracts of poly(dA) but does not interact with polyguanylic, polycytidylic, or polyuridylic tracts. With the short sequences $d(Ap)_X$ ($x = 5-13$) the pentamer $d(Tg)_4$-T-azido forms triple-helical structures with T:A = 2:1; double strands being undetectable in favor of triplex structures.[6a,b] In this study molecular dynamics techniques are applied to obtain the structural insights and better understanding of the interaction of DNG oligomers with DNA. Theoretical simulations of DNA structure have a rich history, as discussed in reviews by Beveridge et al.[12a,b] Nanosecond molecular dynamics simulations with explicit solvent, counterions, and full periodic boundary conditions, as well as Ewald method to overcome the long range convergence problem, have been recently reported on triplex DNA (Weerasinghe et al.[13a]) and on duplex DNA, RNA, and DNA/RNA hybrid without restraints (Cheatham et al.[13b,c]). We had applied these molecular dynamics techniques to the RNG·DNA hybrid duplex eight base pairs in length.[14] This study involves an investigation of molecular dynamics simulations in water of the conformations of $d(Tg)_8d(Ap)_8d(Tg)_8$, a DNG·DNA·DNG hybrid triplex, and $d(Tg)_8d(Ap)_8$, a DNG·DNA hybrid duplex. The results are analyzed to compare with the experiment observation. We have focused on the hydrogen-bonding pattern, the stability, and nature of the hybrid complexes, with special emphasis on the bending and the minor groove narrowing due to electrostatic attraction of DNG and the DNA.

Computational Experiments

Model building and computations were performed on a Silicon Graphics workstation using CHARMM[15a,b] program version 22.5 and Quanta modeling package 4.0 (MSI, Waltham, MA, currently, Biosym/MSI, San Diego, CA). DNG·DNA·DNG triplex hybrid $[d(Tg)_8d(A_p)_8d(Tg)_8]$ and DNG·DNA double helical hybrid $[d(Tg)_8{\cdot}d(Ap)_8]$ were built using a theoretical structure of triple helical DNA $[d(Tp)_{10}d(A_p)_{10}d(Tp)_{10}]$[15c] as a starting point. Guanidinium groups [−NH−C(=N^+H_2)−NH−] were overlapped on the phosphate linkages [−O−(PO_2−)−O−] of the pyrimidine strands; sodium ions were placed adjacent to the phosphate moieties along the purine strand, and chloride ions were placed near the guanidinium groups, by using the method described in previous publications from this laboratory.[1,3,5,14] The solutes were placed in a cubic box of dimensions 35.10 × 34.18 × 33.59 Å^3 with the helical axis parallel to the *z* direction. Water molecules (1791) were placed in the box and those with close contacts to the solute atoms (within 2.6 Å) were excluded from the solution leaving a total of 1467 water molecules in the periodic boxes for the hybrid duplex and 1453 water molecules for the hybrid triplex.

The CHARMM residue topology file DNAH.RTF was used for the standard DNA residues and was modified to use for DNG residues by comparison with DNAH.RTF.[1,3,5,14] All atom CHARMM force field parameters were used in the simulations. Atom types C, NC, and HC were used for the carbons, nitrogens, and hydrogens of the guanidines, respectively. Water molecules were treated as TIP3P residues.[15d] The initial velocities were generated by a Maxwell−Boltzman distribution at a temperature of 300 K. Periodic conditions were applied in all three directions. An accurate representation of long-range electrostatic interactions in MD simulations is extremely important. This is particularly true for highly charged systems, such as DNA and RNA.[16a−c] The Ewald summation method[16d] was used to overcome the electrical static potential convergence problem caused by the cut off due to the excess amount of computation time required for the simulation method used. The assemblies were minimized prior to dynamics runs to remove the strain in the initial structures. One hundred steps of steepest descent algorithm minimization were followed by the adopted basis Newton−Raphson algorithm minimization for

(1) Dempcy, R. O.; Almarsson, O.; Bruice, T. C. *Proc. Natl. Acad. Sci. U.S.A.* **1994,** *91*, 7864.
(2) Dempcy, R. O.; Browne, K. A.; Bruice, T. C. *J. Am. Chem. Soc*. **1995,** *117*, 6140.
(3) Dempcy, R. O.; Browne, K. A.; Bruice, T. C. *Proc. Natl. Acad. Sci. U.S.A.* **1995,** *92*, 6097.
(4) Browne, K. A.; Dempcy, R. O.; Bruice, T. C. *Proc. Natl. Acad. Sci. U.S.A.* **1995,** *92*, 7051.
(5) (a) Dempcy, R. O.; Luo, J.; Bruice, T. C. *Proc. Natl. Acad. Sci. U.S.A.* **1996**, *93*, 4326.
(6) (a) Blaskó, A.; Dempcy, R. O.; Minyat, E. E.; Bruice, T. C. *J. Am. Chem. Soc*. **1996,** *118*, 7892. (b) Blaskó, A.; Minyat, E. E.; Dempcy, R. O.; Bruice, T. C. *Biochemistry* **1997**, *36*, 7821.
(7) Uhlmann, E.; Peyman, A. *Chem. Rev*. **1990**, *90*, 543.
(8) Crooke, S. T. *Annu. Rev. Pharmacol. Toxicol*. **1992,** *32*, 329.
(9) Crooke, S. T. *FASEB J*. **1993**, *7*, 533.
(10) Cook, P. D. In *Antisense Research and Applications*; Crooke, S. T., Lebleu, B., Eds.; CRC: Boca Raton, FL, 1993; pp 149−187.
(11) Sanghvi, Y. S. And Cook, P. D. In *Nucleosides and Nucleotides as Antitumor and Antiviral Agents*; Chu, C. K., Baker, D. C., Eds.; Plenum: New York, 1993; pp 311−324.
(12) (a) Beveridge, D. L.; Swaminathan, S.; Ravishanker, G.; Withka, J. M.; Srinivasan, J.; Prevost, C.; Louise-May, S.; Langley, D. R.; DiCapua, F. M.; Bolton, P. H. In *Water and Biological Molecules*; Westhof, E., Ed.; Macmillan Press: New York, 1993; pp 165−225. (b) Beveridge, D. L.; Ravishanker, G. *Curr. Opin. Struct. Biol*. **1994**, *4*, 246.
(13) (a) Weerasinghe, S.; Smith, P. E.; Mohan, V.; Cheng Y.-K.; Pettitt B. M. *J. Am. Chem. Soc*. **1995,** *117*, 2147. (b) Cheatham, T. E., III; Kollman, P. A. *J. Mol. Biol*. **1996**, *259*, 434. (c) Cheatham, T. E., III; Kollman, P. A. *J. Am. Chem. Soc*. **1997,** *119*, 4805.
(14) Luo, J.; Bruice, T. C. *J. Am. Chem. Soc*. **1997,** *119*, 6693.
(15) (a) Brooks, B. R.; Bruccoleri, R. E.; Olafson, B. D.; States, D. J.; Swaminathan, S.; Karplus, M. *J. Comput. Chem*. **1983**, *4*, 187. (b) MacKerell, A. D., Jr.; Wiorkiewicz- Kuczera, J.; Karplus, M. *J. Am. Chem. Soc*. **1995**, *117*, 11946. (c) Raghunathan, G.; Miles, H. T.; Sasisekharan, V. *Biochemistry* **1993,** *32*, 455. (d) Jorgensen, W. L.; Chandrasekhar, J.; Madura, J. D. *J. Comput. Chem*. **1983**, *14*, 89.
(16) (a) York, D. M.; Darden, T. A.; Petersen, L. G. *J. Chem. Phys*. **1993**, *99*, 8345. (b) Schreiber, H.; Steinhauser, O. *Biochemistry* **1992**, *31*, 5856. (c) Steinbach, P. J. And Brooks, B. R. *J. Comput. Chem*. **1994**, *15*, 667. (d) De Leeuw, S. W.; Perram, J. W.; Smith, E. R. *Proc. R. Soc. London, Ser. A* **1980,** *373*, 27. (e) Ewald, P. *Ann. Phys. (Leipzig)* **1921**, *64*, 253−264.

Chart 2

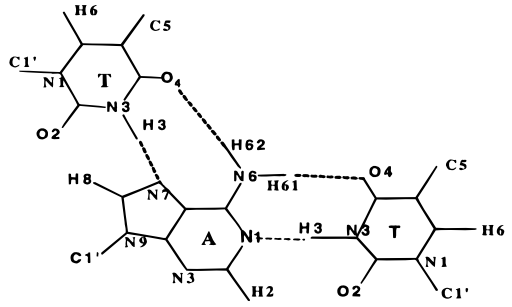

3'	T8	T7	T6	T5	T4	T3	T2	T1	5'
	‖	‖	‖	‖	‖	‖	‖	‖	
5'	A1	A2	A3	A4	A5	A6	A7	A8	3'
	‖	‖	‖	‖	‖	‖	‖	‖	
5'	T1	T2	T3	T4	T5	T6	T7	T8	3'

5000 steps. Nonbonding interactions were cut off at 10 Å. Dynamics for the assembly to 1120 ps (triplex) and 1420 ps (duplex), using a step of 0.001 ps and the SHAKE bond constraints[17] were run using Verlet integration. Hydrogen bonds were not restrained during the simulation since free MD (dynamics without restraints) is a more natural and ideal way of simulation.

The Ewald[16d,e] method derives the electrical static potential to be the sum of real space and reciprocal space contributions (eq 1 and 2), where erfc() is the complimentary error function, V is the volume

$$\Phi_{\text{real}}(\mathbf{r},\beta) = \sum_n \text{erfc}(\beta|\mathbf{r}+\mathbf{n}|)/|\mathbf{r}+\mathbf{n}| \quad (1)$$

$$\Phi_{\text{recip}}(\mathbf{r},\beta) = 1/\pi V \sum_{m\neq 0} \exp(-\pi^2\mathbf{m}^2/\beta^2)\exp(2\pi i\mathbf{m}\cdot\mathbf{r})/\mathbf{m}^2 \quad (2)$$

of the periodic box, and n and m are the real and reciprocal space indices. β is a positive parameter, the value of β adjusts the relative rates of convergence of the real and reciprocal space sums. A heating phase of 3 ps for a final temperature near 300 K was followed by an initial equilibrium of 17 ps and a second phase of equilibration of 500 ps, and finally 600 ps for observance, for the triplex system calculation. For the duplex system, the final observation phase was 900 ps. During the initial equilibration, the velocities were scaled to maintain a temperature near 300 K. To visualize the structural evolution history, trajectory coordinates were saved every 1 ps, giving 1100 and 1400 structures for analysis of the average structure from the last 1100 and 1400 ps, respectively, of MD which represents the second phase equilibration and the equilibrated collection phase.

Results and Discussions

Molecular dynamics runs were performed on the DNG·DNA·DNG triplex hybrid $[d(Tg)_8d(A_p)_8d(Tg)_8]$ and DNG·DNA double-helical hybrid $[d(Tg)_8{\cdot}d(Ap)_8]$ in water with Na^+ and Cl^- counterions, under the periodic boundary conditions using the Ewald summation method for long-range interactions (Computational Experiments section). The molecular dynamics results and statistical analyses were extracted from 1120 and 1420 ps trajectories, respectively, and are based on the 1117 and 1417 sample structures, respectively, after the heating stage of the dynamics run. Detailed results of the simulations and the structural properties of the hybrid duplex and triplex are presented in what follows.

Throughout the 1.12 and 1.42 ns dynamics simulations, and without structural constraints, the hydrogen bondings of the hybrid triplex and duplex structures remained intact (Chart 2). With time, certain DNG strand backbone torsion angles, which describe the geometries around the guanidinium group, change away from the initially assumed standard A-DNA values. This relaxation takes around 400−600 ps for both systems and relieves the tensions due to the replacement of the phosphate by guanidinium groups. After equilibration a new helical geometry was established. For the Hoogstein pairs in the triplex, even the two ends are perfectly hydrogen bonded except one hydrogen bond at 3′ end is extended to 3.8 Å. For the Watson−Crick pairs in triplex, at each end one hydrogen bond is intact, and the other is extended to between 4 and 5 Å in length. In the duplex, at the 3′ end one hydrogen bond is intact, and the other is extended to 3 Å in length; at the 5′ end both hydrogen bonds are extended to 3 to 4 Å in length. Both ends are unraveled in conventional the DNA or RNA duplex and triplex oligomers. However the helical parameters, twist and rise, phase transferred[13b,c] to the neighborhood of a B-DNA frame with few exceptions for the duplex. For the triplex, the twist parameter unwinds to the lower end of an A-DNA value, 28°. But the helical rise of the triplex phase transferred to the high end of a B-DNA value, 3.8 Å. The second base pair next to the 3′ end (A6-T3) showed a certain degree of unwinding and a change in the rise for the duplex. We will discuss this aspect later. Most backbone torsional parameters for the duplex and triplex remained unchanged from the conventional A- and B-DNA backbone values. The β parameter had the most dramatic changes away from A and B values. The torsional angles in the DNA strands in the duplex and the triplex showed more fluctuations than the DNG strands, reflecting that the DNA torsional parameters possess flexibility. Stereoviews of three MD snapshots (in one bending cycle) for the duplex structure are presented in Figure 1. The snapshots for the same time period of the dynamics run for the triplex structure are presented in Figure 2.

Base-Pair Hydrogen-Bonding Pattern. The triplex and duplex hydrogen-bonding patterns are shown in the histograms of Figure 3 and Figure 4, respectively. Figure 3 visualizes for the hybrid triplex the Hoogstein and Watson−Crick hydrogen-bonding distances of O4−H62, H3−N7, O4−H61, and H3−N1, (panel 1 through panel 4 from the left to the right, respectively) from the first to the eighth base pairing (5′ end to 3′ end, bottom to the top) throughout the dynamics run. Figure 4 shows for the hybrid duplex the Watson−Crick hydrogen-bonding distances of H3−N1 and O4−H61 (the left and right panels respectively) from the first to the eighth base pairing (5′ end to the 3′ end, from bottom to the top) throughout the dynamics run. Figures 3 and 4 represent well-maintained Watson−Crick base pairings for the triplex and duplex, respectively, and even better maintained Hoogstein base pairings for the triplex (Figure 3) during the nanosecond dynamics run without restraining. These base pairings are, undoubtedly, stabilized by the mutual attraction of the polycation and polyanion backbones. For both triplex and duplex, the Watson−Crick H3−N1 pair hydrogen bonding at the 5′ end, is extended to around 4 Å; but all the other H3−N1 pairings are bound tightly with vibrational amplitude of 0.3 Å, except for the duplex the Watson−Crick H3−N1 pair hydrogen bonding at the 3′ end is also extended to around 3 Å. And for both systems the base-pair opening and breathing activities are more pronounced in the major groove side for O4−H61 (the Watson−Crick, panel 3) and O4−H62 (the Hoogstein, panel 1 in Figure 3) for the hybrid triplex and O4−H61 (the right panel in Figure 4) for the hybrid duplex. The dramatic openings appear in the central tracks (A5T4 and A6T3 for triplex and A4T5 for duplex) due to bending (and for the Watson−Crick hydrogen bondings for the triplex system and at the major groove sides (O4−H61) for

(17) Van Gunsteren, W. F.; Berendsen, H. *J. C. Mol. Phys.* **1977,** *34,* 1311.

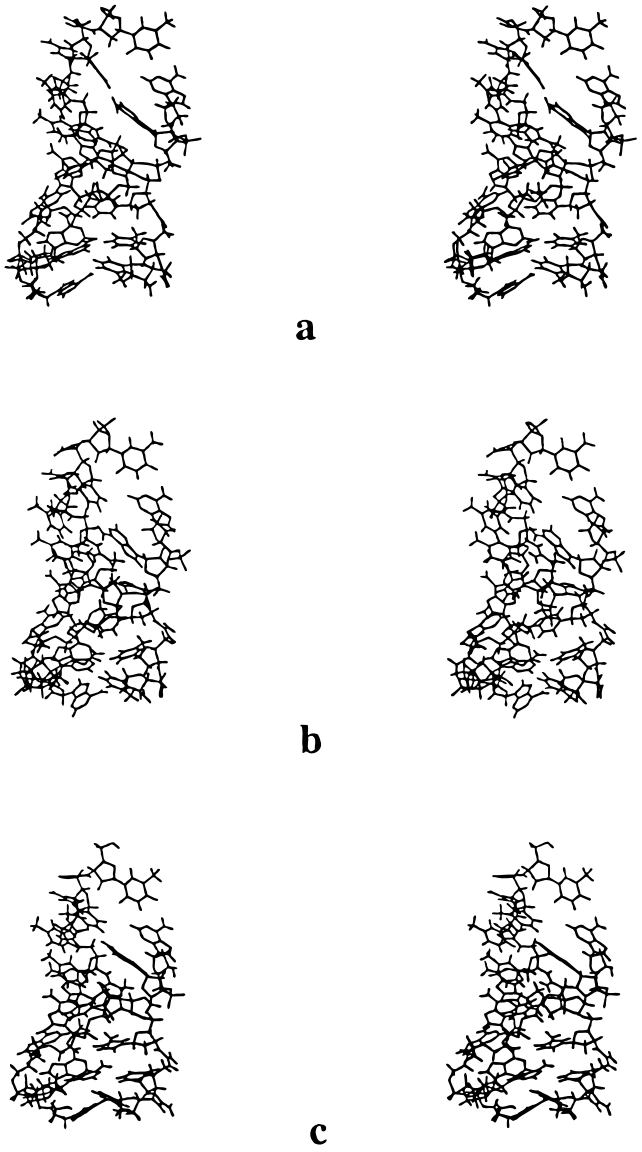

Figure 1. Stereoviews of three MD snapshots of the hybrid duplex with 100 ps intervals.

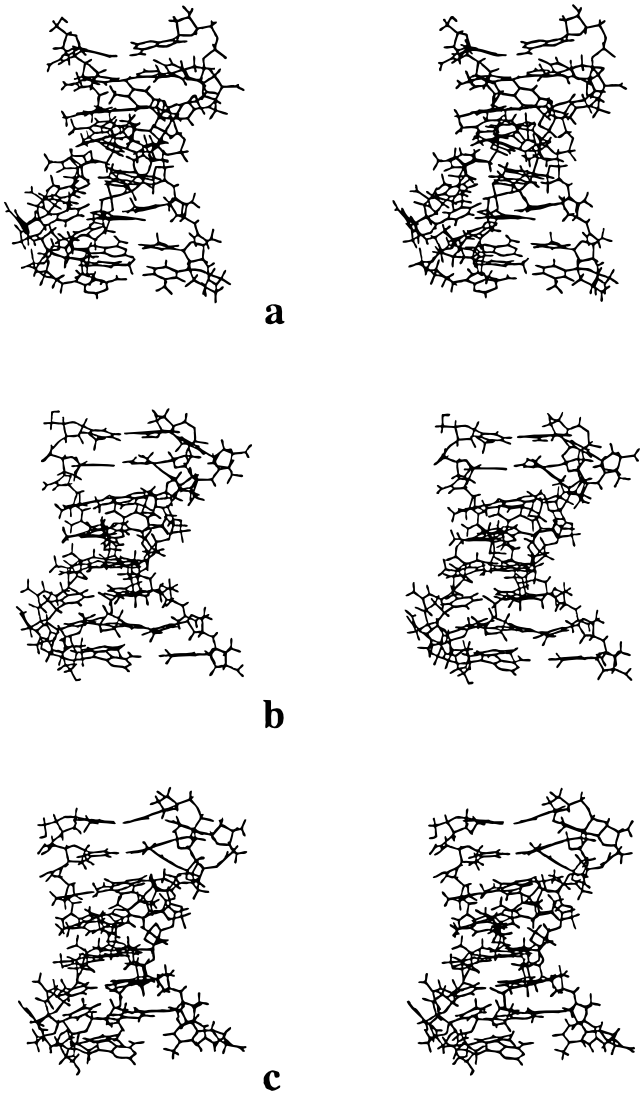

Figure 2. Stereoviews of three MD snapshots of the hybrid triplex with 100 ps intervals.

the duplex system). The Hoogstein pair at the major groove side (O4−H62) has less pronounced motions than the Watson−Crick one. This gives overall stability for the hydrogen bondings of the Hoogstein base pairs (left two panels, O4−H62 and H3−N7) in the triplex. H3−N7 bonds have very confined distances even for the 3′ end. And for the major groove side O4−H62 bonds have more confined distance motions than O4−H61 bonds for the major groove side of the Watson−Crick pairings portion in the triplex structure. It is the Hoogstein pairings in the triplex that make the hybrid triplex more favorable than the duplex. Note that at the 5′ ends, the fraying extent is more pronounced for the hybrid duplex than the triplex. This is another indication that the hybrid triplex structure is more favorable than duplex structure. We previously reported the triplex observation rather than the duplex in our thermodynamic experimental studies.[6a,b]

Three-centered bifurcated (propeller twist) hydrogen bondings[18] are often observed for AT tracts. The high degree of propeller twist helps maximize purine−purine stacking interactions and creates a potential system of additional hydrogen bonds. The extra hydrogen bond will certainly be of greater significance in stabilization of base pairing between the two strands. On the other hand the three centered bifurcated bondings often contribute to the bending of the tract.[18] In our 1120 ps and 1420 ps dynamics trajectories, three centered hydrogen bondings are observed. The bifurcating bond distances with time are presented in Figure 5 for O4-H62 of A2-T6, A3-T5, A4-T4, A5-T3, and A6-T2 (left panel for triplex, right panel for duplex, 5′ end to 3′ end from bottom to top). It is interesting to note that the bifurcatings at the left panel for the triplex were not maintained at the central pairings for A4T4, probably due to the bending and the elongation of the central tract associated with the suggested twist and rise parameters phase transferring to a B conformation in the hybrid triplex structure. However, the Hoogstein pairings and the other bifurcating hydrogen bondings (A2T6, A5T3, and A6T2) help to stabilize the overall structure. For the duplex, we note that only the base pair A2T6 near the 5′ end exhibited bifurcating. This corresponds to the experimental fact that the duplex was not observed at room temperature and at shorter sequence because the duplex is less favorable with less bifurcated hydrogen bondings. The propeller twists associated with these bifurcatings is considered when describing the helical parameters (vide intra).

(18) (a) Nelson, H. C. M.; Finch, J. T.; Luisi, B. F.; Klug, A. *Nature* **1987**, *330*, 221. (b) Coll, M.; Frederick, C. A.; Wang, H.-J.; Rich, A. *Proc. Natl. Acad. Sci. U.S.A.* **1987**, *84*, 8385.

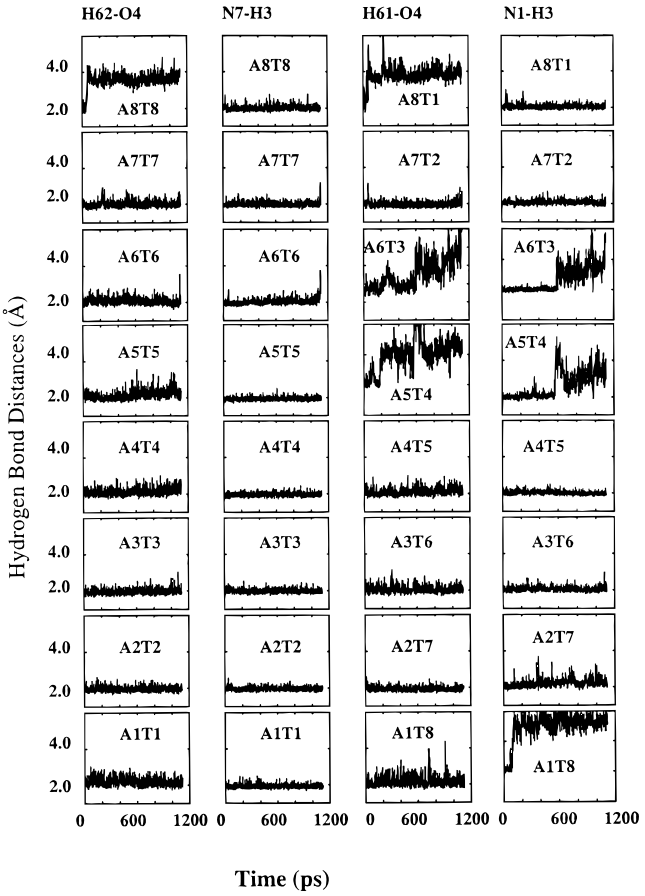

Figure 3. For hybrid triplex, the entire Hoogstein and Watson−Crick hydrogen bonding distances of O4−H62, H3−N7, O4−H61, and H3−N1, (panel 1 through panel 4 from the left to the right, respectively) from the first to the eighth base pairing (5′ end to 3′ end, bottom to the top) throughout the dynamics run.

The Minor Groove Widths. In Figure 6 we present the sample histograms of the phosphate-P−guanidinium-C distances across the minor groove during the dynamics run for the hybrid duplex and triplex. Figure 6a is the histogram of the phosphate-P−guanidinium-C distance across the minor groove of the duplex structure measured from phosphate-P of A7 to guanidinium-C of T6. The histogram shows that attainment of equilibration at the minor groove width took at least about 450 ps. After equilibration the average minor groove width of the duplex measured from phosphate-P of A7 to guanidinium-C of T6 is about 7.2 Å.[19a−c] In Figure 6b (triplex) the histogram of the phosphate-P−guanidinium-C distance across the minor groove measured from phosphate-P of A6 to guanidinium-C of T6, shows that attainment of equilibration at the minor groove width took at least 250 ps. After equilibration the average minor groove width measured from phosphate-P of A6 to guanidinium-C of T6 is about 6.0 Å.[19a−c] The fluctuations in the minor groove widths as shown in Figure 6a and b may well allow minor groove binders, such as the drug distamycin, to enter the minor groove. Tables 1 and 2 record the overall minor groove matrix[19a−c] (phosphate-P−guanidinium -C distances) of the average structure over the dynamics run for duplex and triplex, respectively. The results were obtained using the

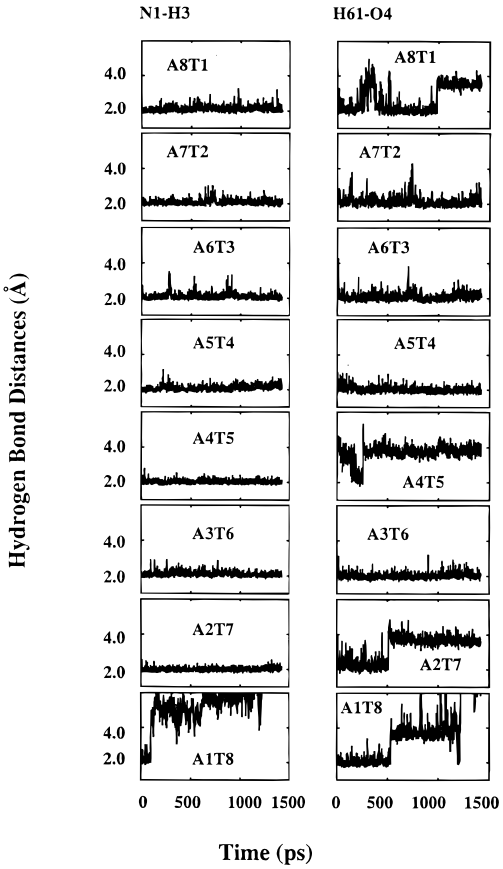

Figure 4. For the hybrid duplex the entire Watson−Crick hydrogen bonding distances of H3−N1 and O4−H61 (the left and right panels respectively) from the first to the eighth base pairing (5′ end to the 3′ end, from bottom to the top) throughout the dynamics run.

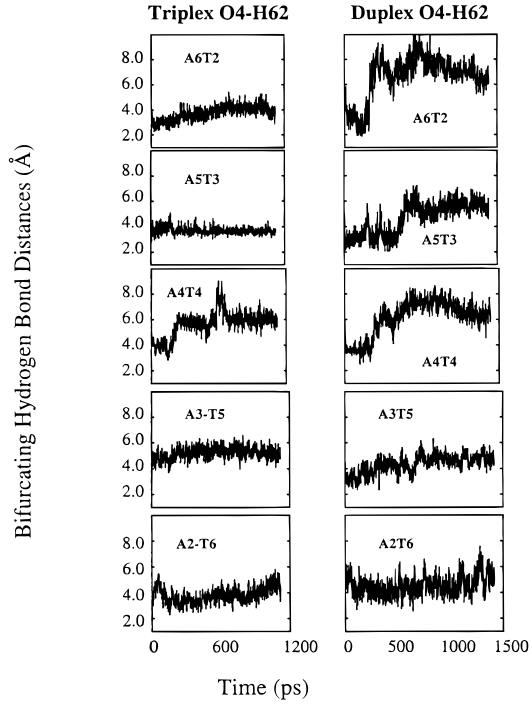

Figure 5. Three-centered bifurcating hydrogen bonding (O4−H62) distance histogram of A2- T6, A3-T5, A4-T4, A5-T3, and A6-T2 (left panel for triplex, right panel for duplex, 5′ end to 3′ end from bottom to top), from time 20 ps to 1120 ps (triplex), and to 1420 ps (duplex).

(19) (a) Conner, B. N.; Takano, T.; Tanaka, S.; Itakura, K.; Dickerson, R. E. *Nature* **1982**, *295*, 294. (b) Dickerson, R. E. *Sci. Am.* **1983**, *249* (6), 94. (c) Minor groove width was defined[19a,b] as the centered atom distance less the van de Waals radius, van de Waals radius is taken as 5.8 Å[19a,b] for the two centered atoms, phosphate-P and guanidinium-C. (d) Prive, G. G.; Yanagi, K.; Dickerson, R. E. *J. Mol. Biol.* **1991**, *217*, 177, (e) Prive, G. G.; Dickerson, R. E.; et al. In Structure & Expression. *DNA & Its Drug Complexes*; Sarma, M. H., Sarma, R. H., Eds.; Adenine Press: New York, 1988; Vol. 2.

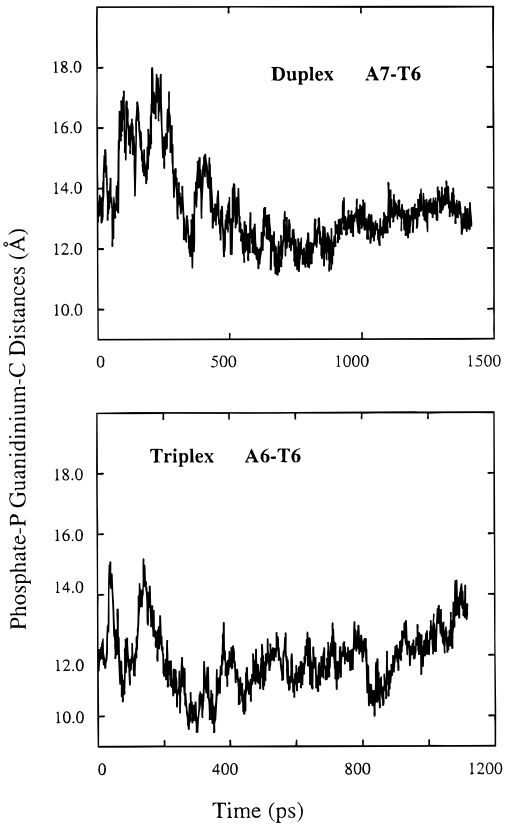

Figure 6. (a) Minor groove width (phosphate-P−guanidinium-C distance) histogram from 20 ps to 1420 ps measured from A7 to T6 across the minor groove for the duplex structure (top). (b) Minor groove width (phosphate-P−guanidinium-C distance) histogram from 20 ps to 1120 ps measured from A6 to T6 across the minor groove for the triplex structure (bottom).

Table 1. Phosphate-P−Guanidinium-C Distance Matrix (Å) for the Duplex

	T2	T3	T4	T5	T6	T7	T8
A2	21.8	17.4	13.2	10.8	11.1	12.0	11.6
A3	18.2	15.0	12.1	10.4	10.2	10.7	9.3
A4	17.5	15.6	14.0	12.8	12.0	11.6	8.9
A5	12.8	11.8	11.4	10.8	10.0	10.3	8.7
A6	11.5	11.5	11.5	10.5	8.8	8.6	7.7
A7	10.4	10.6	10.7	9.2	7.2	7.5	8.8
A8	10.8	10.0	9.2	7.0	5.1	6.9	10.7

Table 2. Phosphate-P−Guanidinium-C Distance Matrix (Å) for the Triplex

	T2	T3	T4	T5	T6	T7	T8
A2	17.6	17.6	17.0	15.6	14.7	13.9	13.4
A3	15.9	16.7	16.6	15.0	13.6	12.1	11.3
A4	13.3	14.5	14.6	13.1	11.7	10.4	10.3
A5	11.5	12.5	12.4	10.8	9.7	9.1	10.2
A6	10.9	10.3	9.1	6.9	6.0	6.6	9.5
A7	10.2	10.0	9.6	8.5	9.0	10.4	13.9
A8	11.8	12.1	12.6	12.7	14.1	16.1	19.7

NEWHELIX 93 program.[19d] In the distance matrixes, the DNA strand runs 5′ to 3′ down from top to bottom with the column representing A2→A8, whereas the DNG strand runs 5′ to 3′ across from left to right with the horizontal line representing T2→T8. By examining the matrix minor groove matrix in Table 1, the shortest phosphate-P−guanidinium-C distances for the duplex across the minor groove are 7.7, 7.5, and 5.1 Å for A6-T8, A7-T7, and A8-T6, respectively. In the triplex structure, the shortest phosphate-P−guanidinium-C distances across the minor groove are 10.3, 9.1, 6.0, and 8.5 Å for A4-T8, A5-T7, A6-T6, and A7-T5, respectively (Table 2). The minor groove widths are measured, from the phosphate-P of the A tract to the closest guanidinium-C of the T tract. It is apparent that the minor groove contraction in the duplex structure (by 0.7 Å) is the result of polyanion and polycation backbone attractions. The contraction of the minor groove of the triplex is also caused by the third strand in the major groove; however, due to the overall elongation of the triple helixes as discussed earlier, the narrowing is canceled by the elongating; the minor groove width of the triplex remains similar as in a regular DNA duplex. The narrowing and elongating processes is also shown in the Figure 6b (the triplex A6−T6 distance histogram). The elongating appears at around 800 ps, which is in agreement with the end-to-end distance histogram presented later for the triplex in Figure 10.

Counterions and Water Spines. For the hybrid duplex system, counterions have diffused away from their counterpartners during the 1420 ps run. The counterions near the two ends are the most remote. Na^+ ions are more than 8.3 Å away from their original counter phosphate-P's, except for the counterions at A3, A4, and A5 which remain within ∼3.5 Å of the starting positions. Cl^-'s are moving slower, and are more than 4.8 Å away from their original counter guanidinium-C's. This is because the atomic mass of Cl^- is higher than Na^+. The counterions at A2 and A5 are exceptions and they remain within ∼3.3 Å of the starting positions. Due to the internal cancellations of overall charge (polyanion DNA strand vs polycation DNG strand), Na^+ and Cl^- are more prone to drift away from an DNG·DNA pair than Na^+ from a DNA·DNA pair.

However for the hybrid triplex system, counterions, Na^+ and Cl^-, have stayed with their counterpartners during the 1120 ps run. With only partial internal cancellations of overall charge (one polyanion DNA strand vs two polycation DNG strands), Na^+ and Cl^- are more prone to stay aligned with their counterpartners. The counterions near the two ends are most remote. Na^+ ions are within 5.0 Å from their original counter phosphate-P's, and for the counterions at A4, A5, A6, and A7 remain within ∼3.5 Å of the starting positions. Cl^-'s are within 5.3 Å from their original counter guanidinium-C's, except the counterions at A8 of Hoogstein strand. Cl^-'s, at T5, T6, and T7 of Hoogstein strand and at T2, T3, T4, T5, and T6 of Watson−Crick strand, remain within ∼3.2 Å of the starting positions. Figure 7a shows the stereoview of the average hybrid triplex structure through the dynamics run.

Spines of hydration for both minor and major grooves are observed in the snapshots of the hybrid duplex and triplex. Water molecules are hydrogen bonded in the major groove with thymine O4 and adenine amino group, and in minor groove with adenine H2 and thymine O2. Parts b and c of Figure 7 are the stereoviews of a snapshot for duplex structure and triplex structure, respectively. Only the minor groove water spines are present. The minor groove of the hybrid duplex is narrowed and there is one string of water molecules (Figure 7b). The minor groove of the triplex is not as narrow, and due to the base opening as discussed earlier, there are two water molecules running along the walls in the central tract of the strands (Figure 7c).[19e] The water molecules are constantly in fast exchange. The residence time of the water molecules at their hydration sites have been reported at the 0.1−1 ns time region by NMR

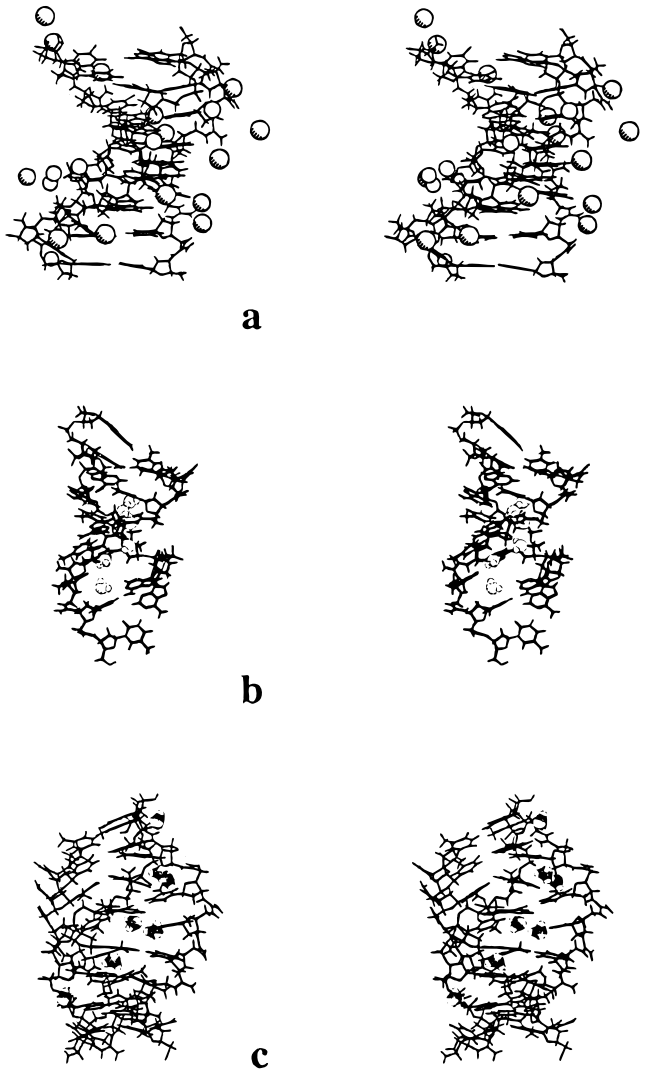

Figure 7. (a) The stereoview of the average hybrid triplex structure with the counterions. (b) The stereoview of a snapshot for duplex structure with the water spine. Only the minor groove water spine is presented. The minor groove of the hybrid duplex is narrowed and there is one string of water molecules. (c) The stereoview of a snapshot for triplex structure with water spine. Only the minor groove water spine are presented. The minor groove of the triplex is not as narrow, and due to the base opening as discussed earlier, there are two water molecules running along the walls in the central tract of the strands.[19e]

experiments[20a,b] for DNA oligomers d(CGCGAATTCGCG)$_2$ and d(AAAAATTTTT)$_2$. In an averaged structure, only those water molecules with a residence time longer than the time span will remain in the hydration sites. Water molecules are not observed in major and minor grooves in both structures averaged over our simulation time span 1 ns. Thus the water spines in minor and major grooves for both structures have lifetimes equal to or less than 1 ns. Structural water molecules mediating protein DNA interactions have been observed in the major groove[20c] by crystallographic studies.

Sugar Puckering. The sugar pseudorotation parameters[21] obtained by use of NEWHELIX 93, are summarized in Supporting Information (Tables 3 and 4 for the hybrid duplex and Watson−Crick pair portion of the triplex respectively).

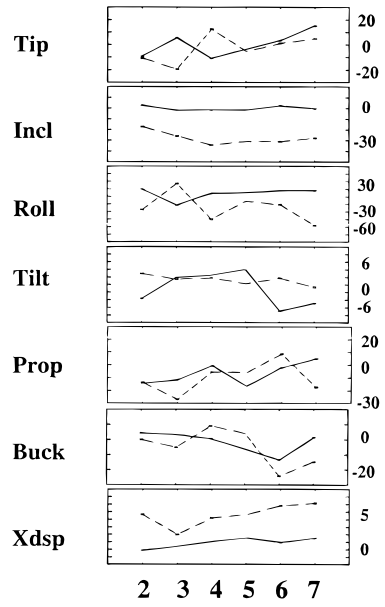

Figure 8. Helical parameters (best plane through both bases) for average duplex (dashed lines) and triplex (solid lines) structures.

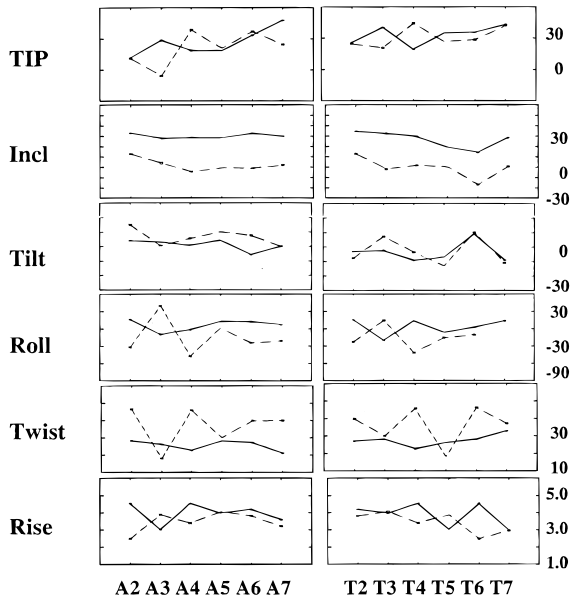

Figure 9. Helical parameters of each strand for average duplex (dashed lines) and triplex (solid lines) structures with A (DNA) strands at left panel and T (DNG) strands at right panel.

Helical, Axis, and Base-Pair Parameters. In flexible systems such as nucleic acids, an apparent conservation of structure over time may be the result of compensatory conformational changes in the systems. The helical rotations and translations parameters involving two bases of a pair or two successive base pairs (best plane through both bases) of the average structures over the 1117 ps dynamics run for the triplex hybrid and over the 1417 ps dynamics run for the duplex hybrid are analyzed and extracted in Figure 8, using NEWHELIX 93 program.[19d] The helical rotation parameters involving each base or two successive bases for each strand of the average structures over the 1117 ps dynamics run for the triplex hybrid and over the 1417 ps dynamics run for the duplex hybrid are analyzed and extracted in Figure 9. The helicoidal description of a nucleic

(20) (a) Liepinsh, E.; Otting, G.; Wuthrich, K. *Nucleic Acids Res.* **1992**, *25* (24) 6549. (b) Otting, G.; Liepinsh, E. *Acc. Chem. Res.* **1995**, *28*, 171. (c) Sigler, P. B. Proceedings of the Robert A. Welch Foundation 37th Conference on Chemical research; Houston, 1993; Chapter 5.

(21) (a) Saenger, W. *Principles of Nucleic Acid Structure*; Springer-Verlag: New York, 1983. (b) McCammon, J. A.; Harvey, S. C. *Dynamics of Proteins and Nucleic Acids*; Cambridge University: Cambridge, 1988. (c) Harvey, C. H.; Prabhakaran, M. *J. Am. Chem. Soc.* **1986,** *108*, 20, 6128.

acid involves a set of parameters.[22] We refer the reader to the references for detailed definitions of the 20 total parameters.[22] At this time we will only emphasize those that are more influential to the overall structural features in our molecules.[14] X displacement (XDP) specifies the displacement of a nucleotide base pair from the helical axis. INC is diagnostic for A- or B-DNA. TIP varies considerably away from 0 in both A and B conformations to negative angles. The variations in TIP are probably due to the substitution of the backbone linker.

The main deviations appear in the buckle (BUCK, the angle of two bases of a base pair) at the hinge points at junction steps, A3−T14, A4−T13, A5−T12, and A6−T11, and where the axis hinge turns direction at the center of the tract, A4−T13. The total angle measured between the local axis vectors of the first and last helical axis segments is about 30° for both the duplex and the Watson−Crick base-pair portion of the triplex structures. A more noticeable parameter is the propeller twist (PRP, the relative rotation between the two bases that are paired). PRP up to −30° is native[22] to the AT base pair of DNA. The AT propeller twist is pronounced because two hydrogen bondings per base pair are less stable than three hydrogen bondings per base pair as in GC pairing. In propeller twist, a third hydrogen bond is obtained from the adjacent base pair. The three centered hydrogen-bonding propeller twist helps to stabilize the hybrid double helix[14] and triple helix. In addition it is found by an energy study[22b] that the base-pair opening process in DNA is greatly facilitated by bending and once a base pair is disrupted by its opening, DNA can bend very easily.

Inspection of Figures 8 and 9 shows the ROL (roll) parameter for duplex structure ranges from −45 to 40°, and for triplex structure, it ranges from −20 to 15°. The RIS parameter (vertical rise of helical bases) is kept at around 3.5 Å for duplex structure and 3.8 Å for triplex structure (typical for a B helix), an exception is at step 2 of the duplex, where the RIS is 2.5 Å. The TWS (helical twist angle per base pair) ranges from 30 to 45° for the duplex and from 20 to 30° for the triplex with an exception at step 5, where the TWS is found as an unwinding value of 18° for the duplex structure. Interestingly, both the unwinding and increased rise help to make room for bending since they provide more space in three dimensions.

Backbone Torsional Angles. Backbone torsional angles were extracted from the average structures over the nanosecond dynamics trajectories. By using the NEWHELIX 93 program,[19d] the numerical values of the torsional angles are obtained and presented in Supporting Information (Figure 11) for the duplex and triplex structure.

Bending Is Accompanied by Strong Bifurcating. The bending features of DNA are important in transcription, replication, recombination, and other processes.[23−35] In Figure 10a and b we present the end-to-end distance histories of the DNA and DNG strands for the triplex and duplex, respectively. Examination of these figures shows that both strands for the duplex and for the Watson−Crick portion of the triplex are, generally speaking, moving at the same pace, which shows that DNA and DNG strands are correlated after the duplex and triplex are equilibrated. The variations in the end-to-end length certainly reflect the helical bending for the duplex.

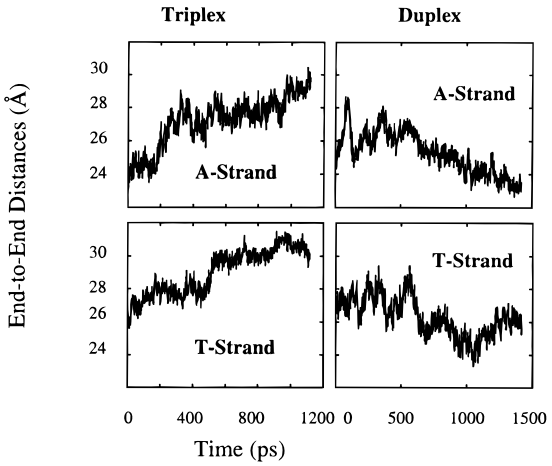

Figure 10. The end-to-end distance histogram for the hybrid triplex (left) and duplex (right) with the A (DNA) strands at the top and T (DNG) strands at the bottom.

Strauss et al.[36] synthesized DNA duplexes in which cytosine bases are modified at the nucleobase 5 position by the addition of an amino group, tethered by a hexamethylene chain. They showed that tethering six ammonium ions on one helical face causes DNA to bend by about 5°. From the helical parameter analyses in our study, using the average structure, we conclude that bending is induced upon substitution of guanidine [−NH−C-(=N^+H_2)−NH−] for phosphate linkages. The bending is obvious on examination of the tip and roll parameters of duplex and triplex structures in Figures 8 and 9, which show a significant macroscopic curvature for both structures. For both duplex and triplex structures the total angle measured between the local axis vectors of the first and last helical axis segment is about 30°. Thus we may conclude that complexing of our DNG to its complimentary DNA in the hybrid duplex and triplex structures enhances the bending capability of the DNA. Our results lend credence to the hypothesis that DNA-binding proteins change the shape of DNA by asymmetric neutralization of phosphate charges.[23−36]

Conclusions

We have performed 1120 and 1420 ps molecular dynamics simulations on the DNG·DNA·DNG triplex hybrid [$d(Tg)_8d(A_p)_8d(Tg)_8$] and DNG·DNA double helical hybrid [$d(Tg)_8$.$d(Ap)_8$] in water with full periodic boundary conditions and Na^+ and Cl^- counterions using the Ewald method. Our results show that Watson−Crick hydrogen bonds and Hoogstein hydrogen bonds in the hybrid triplex, without any restraints, remain intact throughout the simulation. Even the two ends of the triplex

(22) (a) Sarma, R. H. *J. Biomol. Struct., Dyn.* **1988**, *3*, 391. (b) Lavery, R.; Sklenar, H. *J. Biomol. Struct., Dyn.* **1989**, *4*, 655.
(23) Liberles, D. A.; Dervan, P. B. *Proc. Natl. Acad. Sci. U.S.A.* **1996**, *93*, 9510.
(24) Thompson, J. F.; Landy, A. *Nucleic Acids Res.* **1988,** *16*, 9687.
(25) Goodman, S. D.; Nicholson, S. C.; Nash, H. A. *Proc. Natl. Acad. Sci. U.S.A.* **1992**, *89*, 11910.
(26) Hallet, B.; Rezsohazy, R.; Mahillon, J.; Delcour, J. *Mol. Microbiol.* **1994**, *14*, 131.
(27) Goryshin, I. Y.; Kil, Y. V.; Reznikoff, W. S. *Proc. Natl. Acad. Sci. U.S.A.* **1994**, *91*, 10834.
(28) Henriquez, V.; Milisavljevic, V.; Kahn, J. D.; Gennaro, M. L. *Gene* **1993**, *134*, 93.
(29) Nakajima, M.; Sheikh, Q. I.; Yamaoka, K.; Yui, Y.; Kajiwara, S.; Shishido, K. *Mol. Gen. Genet.* **1993**, *237*, 1.
(30) Muller, H. P.; Varmus, H. E. *EMBO J.* **1994**, *13*, 4704.
(31) Milot, E.; Belmaaza, A.; Rassart, E.; Chartrand, P. *Virlogy* **1994**, *201*, 408.
(32) Natesan, S.; Gilman, M. Z. *Genes Dev.* **1993**, *7*, 2497.
(33) Meacock, S.; Pescini-Gobert, R.; DeLamarter, J. F.; van Huijsduijen, R. H. *J. Biol. Chem.* **1994**, *269*, 31756.
(34) Kim, J.; Klooster, S.; Shapiro, D. J. *J. Biol. Chem.* **1995**, *270*, 1282.
(35) Perez-Martin, J.; Rojo, F.; DeLorenzo, V. *Microbiol. Rev.* **1994**, *58*, 268.
(36) Strauss, J. K.; Roberts, C.; Nelson, M. G.; Switzer, C.; Maher, L. J., III. *Proc. Natl. Acad. Sci. U.S.A.* **1996**, *93*, 9515.
(37) Levitt, M.; Warshel, A. *J. Am. Chem. Soc.* **1978**, *100*, 2607−2613 (for Supporting Information).

and duplex structures are only partially frayed. The determination of the helical rise and twist parameters of the average structures from the dynamics runs shows that the hybrid duplex and Watson−Crick portion of the triplex assumed a more B-DNA conformation. However, the sugar pucker and other helical, axis, and base-pair parameters of the two structures equilibrate at a A and B complex conformation, from base to base and base pair to base pair, which suggests a more A-DNA-like overall conformation. The strong Hoogstein hydrogen bondings and the partially maintained three centered bifurcatings in the Watson−Crick pair in the triplex system, as shown in Figure 3, suggest that the hybrid triplex is energetically favored as compared to the duplex. This is in agreement with our previously reported thermodynamic study.[6b] Only triplex structures were observed in solution. However, our earlier MD simulations for the hybrid duplex of polycation ribonucleic guanidine (RNG)[14] showed stronger hydrogen bondings and bifurcated hydrogen bondings in the system as compared to the DNG duplex in this study (Figures 1, 2, and 4 in the earlier MD simulations[14] for the hybrid duplex of RNG vs Figures 4 and 5). Thus the prediction is that in solution the RNG duplex has a better chance of being observed than the DNG duplex. The bending distortion of DNG·DNA duplex is accommodated by a certain degrees of unwinding and change of rise at the step two and step three from the 5′ end to provide more space for the bending distortion. For the triplex structure, the bending is mostly accommodated by the rises. Due to the electrostatic attractions between DNA polyanion and DNG polycation, the overall structure of the hybrid complex is more compact than a DNA complex. The most notable structural features are the overall tracts bending to both duplex and triplex structures and the minor groove width narrowing (0.7 Å) compared to the similar DNA duplex. The narrower minor groove induces a wider major groove. This provides more accommodating space, than in a usual DNA duplex, for a third strand forming a triplex. The bending angle measured between the local axis vectors of the first and last helical axis segments is about 30° for the averaged hybrid duplex and triplex structures. Propeller twist up to −30° (associated with three centered hydrogen bonding, helping the stabilization of the hybrid double helix) native to DNA AT base pairing, was also observed for the hybrid duplex and triplex structures. For the triplex, due to the third strand stabilization and elongation, the narrowing is canceled by the elongating; the minor groove width of the triplex remains similar as in a regular DNA duplex. Most backbone torsional parameters remained unchanged from the conventional A- and B-DNA backbone values. Certain DNG backbone torsion angles around the guanidinium group change away from the initially assumed standard A-DNA values to relieve the tensions due to the replacement of the phosphate. However, more importantly, a helical geometry was reestablished with base-pair hydrogen bonding to the DNA strand (sequence recognition), after the equilibration. Water hydrations are observed during the dynamics runs for both hybrid duplex and triplex structures in both minor and major grooves. The counterions, Na^+'s and Cl^-'s, remain in their positions through the dynamics run for the triplex system.

Acknowledgment. This work was supported by the National Institute of Health. We express our gratitude to ONR for support of our computer facilities and NIH for the Supercomputing hours at Frederick Biomedical Supercomputing Center.

Supporting Information Available: Descriptions of sugar puckering and backbone torsional angles (5 pages). See any current masthead page for ordering instructions and Web access instructions.

JA973337I